Nuclear Inst. and Methods in Physics Research, A 878 (2018) 88–98

Contents lists available at ScienceDirect

Nuclear Inst. and Methods in Physics Research, A

journal homepage: www.elsevier.com/locate/nima

X-ray phase-contrast imaging

Marco Endrizzi

Department of Medical Physics and Biomedical Engineering, University College London, Gower Street, London WC1E 6BT, United Kingdom

ARTICLE INFO

Keywords:
X-ray
Phase-contrast
Imaging

ABSTRACT

X-ray imaging is a standard tool for the non-destructive inspection of the internal structure of samples. It finds application in a vast diversity of fields: medicine, biology, many engineering disciplines, palaeontology and earth sciences are just few examples. The fundamental principle underpinning the image formation have remained the same for over a century: the X-rays traversing the sample are subjected to different amount of absorption in different parts of the sample. By means of phase-sensitive techniques it is possible to generate contrast also in relation to the phase shifts imparted by the sample and to extend the capabilities of X-ray imaging to those details that lack enough absorption contrast to be visualised in conventional radiography. A general overview of X-ray phase contrast imaging techniques is presented in this review, along with more recent advances in this fast evolving field and some examples of applications.

Contents

1. Introduction

The use of X-rays for imaging the internal structure of samples quickly spread around the world soon after the first X-ray radiograph was taken by Wilhelm Conrad Röntgen towards the end of 1895 [1]. Great improvements have constantly been made throughout the last century both with regard to the X-ray generators and to the image receptors, including transformative advances such as the introduction of tomography [2]. X-ray imaging is nowadays a standard tool in many diverse fields and disciplines, ranging from medical sciences to materials engineering and including quality control in industry as well as security screening.

Despite tremendous progress, the fundamental working principle has remained unchanged for over a century: contrast is generated by differences in the absorption of the X-rays within the sample. This can provide excellent results when relatively high attenuation exists, but leads to poor image quality when the sample is weakly absorbing. Generally speaking, this occurs for materials and tissues composed of light elements. The possibility of performing phase-based imaging bears

E-mail address: m.endrizzi@ucl.ac.uk.

http://dx.doi.org/10.1016/j.nima.2017.07.036
Received 6 May 2017; Received in revised form 4 July 2017; Accepted 19 July 2017
Available online 31 July 2017
0168-9002/

the potential of making visible what would be undetectable with the conventional method for these classes of samples.

A number of reviews is already available on this topic, including a focus on the evolution and relative merits of these imaging techniques [3], on the transition from synchrotron to conventional sources [4], on medical applications [5–7] with the translation towards clinical implementation [8] the imaging of the breast [9], and also on materials science applications [10,11].

The aim of this review is to present a general overview of the essentials X-ray phase-contrast imaging techniques in the hard X-ray regime, as well as some examples of use in applied investigations. An in-depth discussion is dedicated to the principles and recent advances of edge illumination, a technique that has been intensively investigated in the recent time by our group for the translation of these advanced X-ray imaging techniques into table-top instrumentation that can be compatible with clinical or industrial environments.

2. Methods

X-ray imaging is a general term that embraces an extremely wide set of techniques that are used to produce a representation of the sample under inspection. In order to describe phase-contrast X-ray imaging techniques, we will start from the basis of the more conventional, or absorption-based, approach.

2.1. Absorption imaging

The sketch in Fig. 1 reports the arrangement that is typically used in radiography by using an X-ray source and an image receptor. It is a transmission-type imaging modality in which the image receptor looks at the source and through the sample. The internal structure of the sample can be inspected in this way because the differences in the attenuation of the X-rays, along their trajectories from the generator to the receptor, produce contrast. In order to quantify this effect we will use a two dimensional representation of a simple object, a sphere made of a single material embedded into another homogeneous material. This situation is depicted in Fig. 2 where panel 2a shows the arrangements of X-ray radiation, phantom and detector while the panel 2b the resulting image. The coordinate system is defined as follows: the X-rays propagate from the source along the z axis, the object extends in all the three dimensions and the image at the receptor is a two dimensional distribution of intensity in the (x, y) plane. By using monochromatic radiation of wavelength λ, the intensity at the detector can be described by using the Beer–Lambert law [13]

$$I(x,y) = I_0(x,y)\exp\left[-(\mu_o^\lambda - \mu_h^\lambda)T_o(x,y)\right] \tag{1}$$

where $T_o(x, y)$ is the projected thickness of the object on the (x, y) plane and $I_0(x, y)$ is the intensity incident on the sample. For the simple case presented above this can be calculated analytically. Let us assume a sphere of radius r and centred in the origin. The projected thickness of the sphere, measured by a line profile running across the centre of the sphere ($y = 0$), is given by the real part of

$$T(x) = 2\sqrt{r^2 - x^2}. \tag{2}$$

We can then calculate the corresponding intensity profile by using Eq. (1). In order to do so we need to specify the working energy (30 keV), the materials (aluminium for the sphere and water for the embedding material) and we further assume a constant incident intensity $I_0(x, y) = 1$.

It is often the case, for example when using conventional laboratory sources such as X-ray tubes, that the radiation is polychromatic and its spectrum extends over a range of several tens of keV. This can be included in Eq. (1) by an integration over the energy that takes into account the energy dependence of the source spectrum $I_0(\lambda)$, of the attenuation coefficient μ^λ and of the detector response $D(\lambda)$

$$I(x,y) = \int d\lambda\, I_0(x,y;\lambda)\exp\left[-(\mu_o^\lambda - \mu_h^\lambda)T_o(x,y)\right] D(\lambda). \tag{3}$$

Each monochromatic component of the X-ray beam contributes independently to the contrast, with a weight that is equal to the relative probability of emission and detection, and with the attenuation coefficient characteristic of that particular energy (for example see [14]).

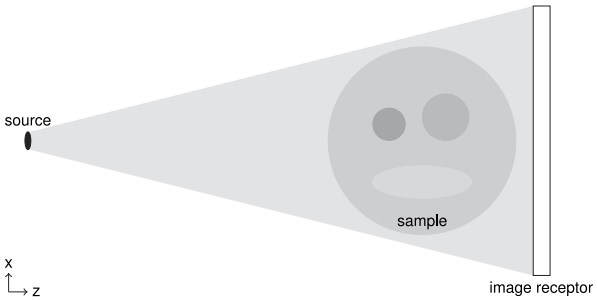

Fig. 1. Schematic of the set-up for conventional X-ray imaging: the image receptor looks directly at the radiation source and through the sample.

2.2. Phase-contrast imaging

The phase of the waves travelling through the sample contributes to the modulation of the detected intensity in an X-ray phase-contrast imaging system. This can be described by means of the complex refractive index [15]

$$n = 1 - \delta + i\beta \tag{4}$$

where the decrement to unity δ governs the phase shifts while β the absorption. Away from absorption edges, and in the region where the photoelectric effect dominates absorption, δ and β can be expressed as functions of the electron density ρ and of the radiation wavelength in the following way [16]

$$\delta(\lambda) = \rho\frac{r_e\lambda^2}{2\pi} \tag{5}$$

$$\beta(\lambda) = \mu(\lambda)\frac{\lambda}{4\pi} \tag{6}$$

where r_e is the classical electron radius. It is worth noting that δ is typically larger than β. By taking for example water at 30 keV, we obtain $\delta \approx 2.56\cdot 10^{-7}$ and $\beta \approx 1.36\cdot 10^{-10}$. Another key difference between the two parameters is their dependence on the X-ray energy E: β decreases approximately with E^{-4} while δ approximately as E^{-2}. Real and imaginary parts of the complex refractive indices of two materials, one composed of light elements and one composed of heavier elements, are plotted in Fig. 3 in the energy range between 10 and 120 keV for illustration purposes.

The phase shift imparted by the sample to the X-ray wave is given by

$$\Phi(x,y;\lambda) = -k\int_{\mathcal{O}} dz\,\delta(x,y,z;\lambda) \tag{7}$$

where the integration is carried out over the extent of the object $\mathcal{O}$ along the optical axis, and this Equation can be considered valid for propagation through thin objects, for which the projection approximation holds [15].

Referring to previous example of a simple sphere composed of a single material, the transmission and phase shift of the sample become

$$I(x,y;\lambda) = \exp\left[-\frac{4\pi\beta(\lambda)}{\lambda}T(x,y)\right] \tag{8}$$

$$\phi(x,y;\lambda) = -k\,\delta\,T(x,y) \tag{9}$$

where a single energy was used for the X-ray beam.

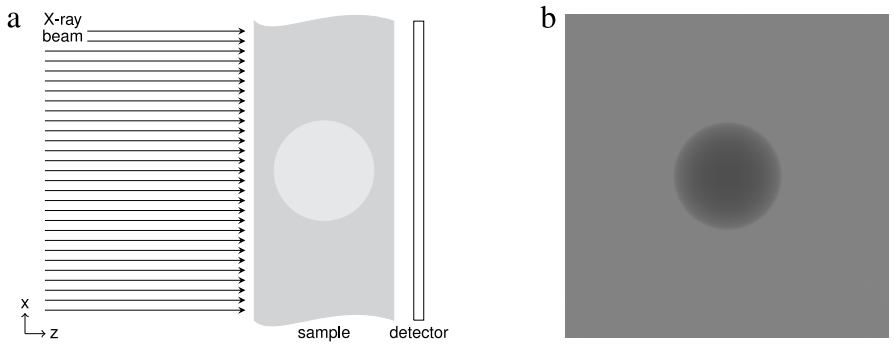

Fig. 2. (a) Simple model for the generation of contrast in absorption-based X-ray imaging. (b) corresponding image recorded represented as the two dimensional distribution of intensity, which was computed by using the X-Tract software [12].

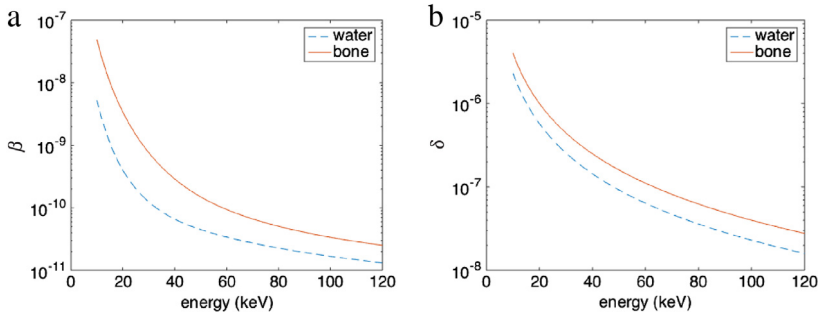

Fig. 3. Complex index of refraction for water and bone as a function of X-ray energy: (a) β and (b) δ. Bone composition was taken from the ICRU report [17].

3. X-ray phase-contrast imaging

It is not possible to directly measure the phase of electromagnetic waves at optical frequencies and above, however, phase effects can play a significant role in the image formation also in the hard X-ray regime. Phase-contrast imaging techniques exploit the phase perturbations introduced by the sample to modulate the intensity recorded at the image receptor, in such a way that these effects can be detected and interpreted.

A summary of these techniques will be presented in the following sections. The classification is inevitably made afterwards, and it is therefore natural that the categories will be appropriate in certain cases while less accurate in others. X-ray phase-contrast imaging techniques are evolving fast, and a large degree of contamination often exists across different approaches. A classification based on the most prominent characteristics of the experimental set-ups and their working principles was chosen here as the main criterion for distinction between different approaches.

3.1. Interferometry

The first example of X-ray phase-contrast imaging method is the X-ray interferometer [18,19] which was built form a monolithic crystal and used a Laue–Laue–Laue configuration. A schematic representation of this device is shown in Fig. 4. Phase-coherent beams are formed by dividing the incoming X-ray beam at the beam splitter S and successively at the transmission element M, they meet again at the analyser A where an atomic-scale standing wavefield is formed [20]. In an ideal scenario, where the wave is perfectly planar and the crystal free of imperfections, the field would be perfectly uniform until a sample is introduced in one of the arms of the interferometer. The image would then record the phase changes induced by sample, modulo 2π. In practice, local phase shifts, arising for example from strain and defects in the crystal, will generate interference patterns that will be superimposed to the modulations imposed by the sample. It is also possible to insert a known phase modulation in one arm, as for example a linear phase ramp

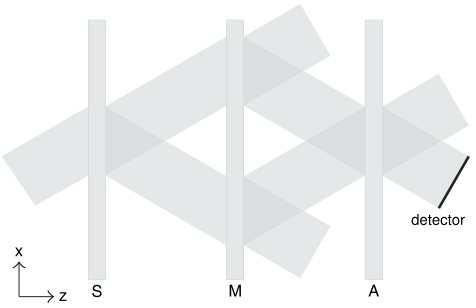

Fig. 4. Top view of an X-ray interferometer.

imposed by using a wedge, while the sample under study is placed in the other arm. The linear phase ramp will generate a series of linear fringes in the intensity recorded at the detector, hence the name of fringe scanning method [21].

Following the first demonstration of the working principle and pioneering imaging experiments [22,23], this method was used for biomedical imaging experiments [24–27] to study different tissue types such as breast, brain and blood [28–30].

3.2. Free-space propagation

Free-space propagation techniques are perhaps the ones requiring the simplest set-up because the introduction of an appropriate propagation distance R_2 between the sample and the image receptor can be sufficient to make phase effects detectable (see Fig. 5). Early works demonstrating this possibility date back to the mid '90s and used both monochromatic and collimated synchrotron radiation [31,32] and polychromatic radiation from a microfocus X-ray tube [33]. This phenomenon can be interpreted in terms of Fresnel diffraction and key features of this approach to imaging can be identified by referring to the

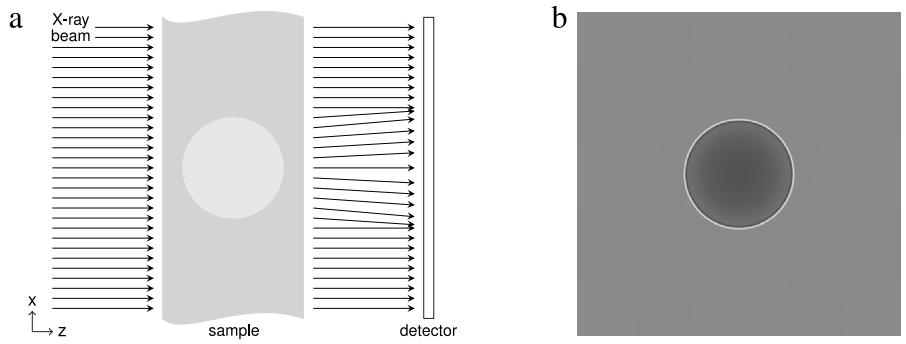

Fig. 5. (a) Simple model for the generation of a phase contrast image with the free space propagation technique. (b) corresponding image recorded represented as the two dimensional distribution of intensity, calculated by using the X-Tract software [12].

following expression [15,33,34]

$$I(x,y;M,\lambda) = \frac{I_0}{M^2}\left[1 + \frac{R_2\lambda}{M2\pi}\nabla_\perp^2\phi(x,y;R_1,\lambda)\right] \tag{10}$$

that describes the intensity distribution at the image receptor plane from a pure phase object. $M = (R_1+R_2)/R_1$ is the geometrical magnification. The contrast from a pure phase object vanishes when $R_2 \to 0$, which is the typical condition for conventional (contact) radiography and the phase term is directly proportional to the propagation distance R_2. Another feature of interest is that the monochromaticity of the radiation is not essential for this type of imaging. A necessary condition, however, is that the radiation must have a certain degree of spatial coherence [13]:

$$l_c = \frac{\lambda R_1}{\sigma_s 2\sqrt{2\log 2}} \tag{11}$$

where σ_s is the standard deviation of the source intensity distribution. The coherence length l_c has to be comparable to or larger than the inverse spatial frequency of the feature of interest [35] in order to obtain significant phase contrast. In practice this means that the source has to be relatively small or that the object must be placed at a relatively large distance R_1 from it. Another requirement is that the imaging system must have spatial resolution high enough to not wash out the interference fringes. This is conveniently summarised by the following expression [36,37]

$$\sigma_t^2 \approx \left(1 - \frac{1}{M}\right)^2\sigma_s^2 + \frac{\sigma_d^2}{M^2} + \sigma_m^2 \tag{12}$$

where σ_t and σ_d are the standard deviations of the system's and of the detector's point spread function, respectively. Another point to be noted is that the diffraction term

$$\sigma_m = \frac{1}{2}\sqrt{\frac{\lambda R_2}{2}} \tag{13}$$

becomes less significant for increasing X-ray energies.

The intensity projection image, acquired with a certain propagation distance between the sample and the detector, will contain a mixture of contributions from both the absorption and the phase shifts in the sample. Other experimental parameters, like the X-ray energy, the geometrical magnification, the radiation coherence and the system resolution, determine the modulation of intensity at the detector. The process that aims at making this type of imaging quantitative by calculating phase and amplitude at the exit surface of the sample is called phase retrieval. Methods to achieve this, in the case of non-interferometric hard X-ray imaging techniques, started developing soon after the first experiments [38–41], also including polychromatic X-ray beams [42] and even exploiting different energies for the phase retrieval process itself [43]. Quantitative retrieval algorithms are also a fundamental component for accurate three-dimensional reconstructions [44–46]. In general terms, the determination of both amplitude and phase requires more than a single measurement (for example by changing the propagation distance or by changing the energy) unless some constraints can be imposed on the sample. Quantitative phase retrieval can be performed from a single defocus distance by requiring homogeneity of the sample [47]: although this might not always be strictly satisfied, it is a very reasonable approximation in many cases of interest (e.g. soft tissue samples) and this approach often delivers high quality projections and reconstructions.

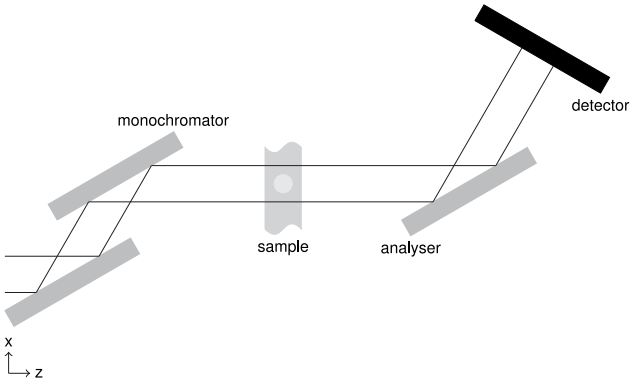

Fig. 6. Example of analyser based imaging set-up.

Applications of free-space propagation X-ray phase-contrast imaging are vast and definitely too many to be covered here. We will limit this discussion to few highlights like micro- and nano-tomography applications [48–54], lung imaging [55–59] and breast tissue imaging [60,61] including in-vivo [62–64].

3.3. Analyser based imaging

Analyser-based methods make use of crystals both for beam preparation and analysis. The crystal arrangement preceding the sample is used to monochromatise and collimate the incoming X-ray beam while the one preceding the detector serves as a fine angular filter. A typical synchrotron experimental set-up is sketched in Fig. 6. The X-ray beam is usually wide enough to cover the extent of the sample along the x direction while scanning along y is often necessary to build a two-dimensional image. The intensity at the detector is modulated by changing the angle of incidence of the X-ray beam on the second (analyser) crystal (see Fig. 7a). This characteristic curve takes the name of rocking curve and it is key in the image formation process. It results from the combination of the reflectivity curves of both the monochromator and the analyser crystal with a contribution arising from the beam divergence [65]. When the system is tuned in such a way that roughly half of the intensity reaches the detector (at full width half maximum of the rocking curve), small changes in the direction of the propagation of the X-rays due to refraction in the sample are

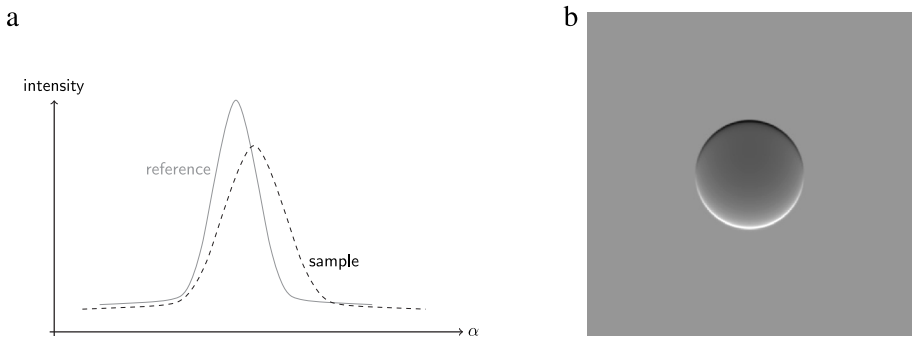

Fig. 7. Image formation principle in an analyser-based system. (a) typical rocking curve: intensity recorder at a fixed position in the detector plane as a function of the "rocking" angle α of the analyser crystal. (b) intensity recorded at the detector when the analyser crystal is set at fixed angle, in such a way that 50% of the intensity is transmitted (obtained by using the X-Tract software [12]).

transformed into intensity changes at the image receptor. The change in direction of propagation is directly proportional to the gradient of the sample's phase [13]

$$\theta_R = \frac{\lambda}{2\pi}\frac{\partial\phi(x,y)}{\partial x} \tag{14}$$

and an imaging system where contrast is proportional to the refraction angle is often referred to as differential phase-contrast imaging system. The image recorded in the case of the sphere sample is shown in Fig. 7b. The X-rays going through the centre of the sphere experience little or no refraction at all, therefore their direction of propagation is not changed and they are transmitted by the analyser with the same probability of the radiation that is not hitting the sample. The image contrast in this region of the sample is mainly due to X-ray absorption within the sample. Refraction increases while approaching the sphere's edges, where the change in the direction of propagation is maximum. Because X-rays are deflected away from the beam axis (a glass sphere in air acts as a diverging lens in the X-ray regime), the angle of incidence of the radiation on the analyser will be changed in two opposite ways at the two edges of the sphere. On one side, this will result in a higher probability of transmission through the analyser, while it will translate into a smaller transmission probability on the opposite side. This is the mechanisms at the basis of the generation of the dark and bright fringes of Fig. 7b.

Early implementations of this technique for imaging fusion pellets are those of Goetz and Forster [66,67]. This approach became increasingly popular after 1995 [68,69] when methods to quantitatively separate phase and absorption contributions were developed [70,71]. This method is intrinsically sensitive to the phase gradient in a single direction only and an additional measurement is typically required to quantify the other component [72]. Another key development that soon followed was the possibility to quantify the effect of the scattering in the sample on the width of the rocking curve, which was put in relation to sub-pixel scale features [73–77]. This was also extended for applications to tomography [78]. Methods for retrieving phase information from the simultaneous acquisition of two images have been developed for the case of Laue analyser [79].

Some examples of the many applications of analyser based techniques in the medical field [80] are: cartilage [81–83], musculoskeletal [84] and breast tissue [65,85–87] imaging and dynamic tracking of micro-bubble concentrations [88,89].

3.4. Grating based imaging

Grating-based imaging methods make use of periodic structures to condition and analyse the X-ray beam. A typical embodiment of this technique is sketched in Fig. 8a where the X-ray beam traverses the sample that modulates its amplitude and imposes phase shifts. It is then passed through the phase grating G_1 and analysed by the absorption grating G_2 immediately before the image receptor. If one of the two grating is laterally scanned (along x) without the sample in the beam, a modulated intensity curve is detected in each pixel. This is often referred to as the phase-stepping curve. When the sample is present in the beam, this curve is modified in three ways, as depicted in Fig. 8b. The relative reduction of the baseline is the conventional absorption image, the lateral shift of the curve represents the differential phase contrast and the reduction of visibility is linked to the scattering in the sample, or dark-field imaging. This can be expressed quantitatively by writing the intensity oscillations recorded at a point (x, y)

$$I(\bar{x};x,y) = \sum_i a_i(x,y)\cos\left(\frac{2\pi i\bar{x}}{p_2} + \boldsymbol{\Phi}_i(x,y)\right) \tag{15}$$

$$\approx a_0(x,y) + a_1(x,y)\cos\left(\frac{2\pi i\bar{x}}{p_2} + \boldsymbol{\Phi}_1(x,y)\right) as \tag{16}$$

where p_2 is the period of G_2 and a_i and $\boldsymbol{\Phi}_i$ are the amplitude and phase coefficient, respectively. The images of the sample are reconstructed by comparing the phase-stepping curves recorded without ^{w} and with ^{o} the sample in the beam [90]. The transmission image, analogous to the one obtained in conventional radiography, is given by

$$T(x,y) = a_0^o(x,y)/a_0^w(x,y). \tag{17}$$

The differential phase-contrast projection image of the sample is calculated by taking the difference $\nabla_x\phi(x,y) = \nabla_x^o\phi(x,y) - \nabla_x^w\phi(x,y)$, and by considering that

$$\nabla_x\phi(x,y) = \frac{p_2}{\lambda d}\boldsymbol{\Phi}_1(x,y) \tag{18}$$

where d is the distance between G_1 and G_2. Dark-field images are obtained by first computing the normalised oscillation amplitude

$$V^w(x,y) = \frac{I_{max}^w(x,y) - I_{min}^w(x,y)}{I_{max}^w(x,y) + I_{min}^w(x,y)} \tag{19}$$

$$= \frac{a_1^w(x,y)}{a_0^w(x,y)} \tag{20}$$

and then by taking the ratio of this quantity, with and without sample in the beam

$$V(x,y) = \frac{V^o(x,y)}{V^w(x,y)} \tag{21}$$

$$= \frac{a_1^o(x,y)a_0^w(x,y)}{a_1^w(x,y)a_0^o(x,y)} \tag{22}$$

which does not show changes ($V(x,y) = 1$) for samples with negligible or absent small-angle scattering and is reduced ($V(x,y) < 1$) when scattering occurs.

Introduction of grating-based techniques could be dated back to early '90s [91,92] with experiments following few years later [93–97]. A breakthrough for the diffusion of this technique was the introduction of a third grating that enabled the use of low brilliance sources [98], tomography [99] and dark-field [100] or scattering imaging were also

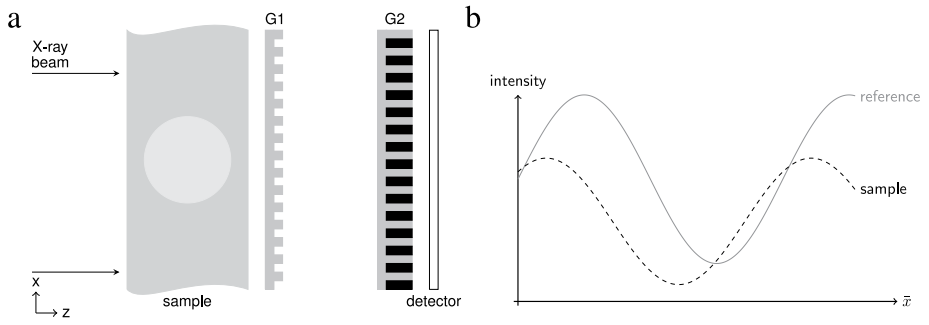

Fig. 8. Example of grating based imaging set-up. (a) typical arrangement where the phase grating is placed after the sample and the (analyser) amplitude grating immediately precedes the detector. (b) intensity recorded at a fixed (x, y) position in the detector plane as a function of the scanning position of one grating relative to the other, along the x direction.

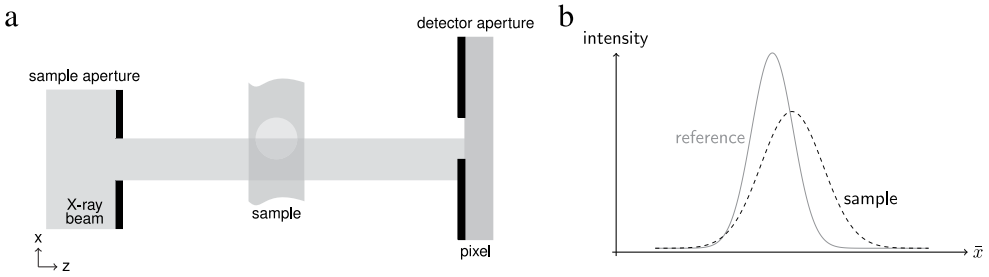

Fig. 9. Edge illumination working principle: (a) typical synchrotron set-up and (b) illumination function.

developed soon afterwards with a three-grating setup. An alternative method was subsequently proposed for differential phase-contrast imaging with weakly coherent hard X-rays [101]. Quantitative three-dimensional dark-field imaging was then developed for these grating-based imaging set-ups [102,103]. The simultaneous determination of the two components of the phase gradient, by means of gratings structured in two dimensions, has also been discussed [104–107]. Another important development is the inverse geometry [108] which can enable compact Talbot–Lau interferometry setups [109]. A much more detailed review of advances and milestones of grating-based X-ray phase-contrast imaging can be found in a recent review [90]. A recent and very promising development on this front was the successful fabrication of grating structures with approximately one order of magnitude finer pitch [110] and their application for the enhancement of table-top imaging systems [111]. Albeit based on gratings, the working principle of this approach is different from that of the more conventional grating-based interferometry and it is best understood under the concept of universal moiré effect [112]. This eliminates the need for an absorption grating and enables the realisation of a polychromatic far-field interferometer that can overcome the limitations in sensitivity and dose efficiency of more conventional bench-top interferometers [112].

An extremely wide spectrum of application exists also for grating based imaging techniques, examples are: breast tissue [113–115], brain tumour [116], cartilage [117–120], and lungs [121,122]. A fairly recent review exists that is fully dedicated to this topic [123].

3.5. Tracking based methods

Another broad category of X-ray phase-contrast imaging techniques stems from the observation that it is possible to measure the sample absorption, refraction and scattering by imposing a known structure to the radiation field and by directly tracking its modifications. In general terms, an overall reduction of the structured beam intensity can be traced back to absorption of the radiation within the sample, while the spatial distortions of the known intensity patterns are used to infer the phase shifts imposed by the sample to the wavefront.

The introduction of this approach may be traced back to the ‘90s [124,125] with experiments following several years later. The structuring could be imposed by using a lenslet array [126], a microprobe [127], an absorption grid [128–130], a phase grating [131] or a speckle pattern [132,133] and the distortions imposed by the sample can be tracked by using a high-resolution detector, also in combination with sub-pixel resolution analysis [134] or by using Fourier-based analysis [135]. These approaches can be extended to two-dimensional sensitivity [136–138], to include dark-field contrast [139,140] and directional dark-field imaging [141–143]; as well as three-dimensional imaging with tomography [142,144].

Applications of tracking based techniques include: bone imaging [145], dynamic airways imaging [146,147] and metrology [142,148,149].

4. Edge illumination

Edge illumination X-ray phase-contrast imaging has been investigated in the recent years as a possible way forward for the translation of phase-sensitive imaging techniques into mainstream applications. Edge illumination was initially developed in synchrotron experiments at Elettra (Italy) and was inspired by analyser-based methods [150]. The typical experimental set-up is reported in Fig. 9a. A beam of synchrotron radiation, propagating from left to right, is shaped down to a narrow blade of radiation by an aperture. It then traverses the sample and impinges on the edge of a second aperture that is placed in front of the image receptor. If one of the two apertures is laterally shifted (along x) the recorded intensity is modulated: it reaches a maximum when the two apertures are perfectly aligned and it progressively decreases for increasing lateral shifts (see Fig. 9b). This is often called illumination function and characterises the properties of this type of imaging systems.

The working principle of edge illumination can be explained by observing that refraction in the sample results in lateral shifts of the X-ray beam which are translated into intensity modulations by the presence of the second aperture. Referring to Fig. 9a, a deflection upwards will result in an increased intensity at the detector pixel while a decreased intensity would be recorded if the deflection occurs downwards. This holds for a completely transparent object that only perturbs the phase of the X-ray beam. If the sample is also absorbing, then at least two images have to be acquired to extract the sample’s absorption and

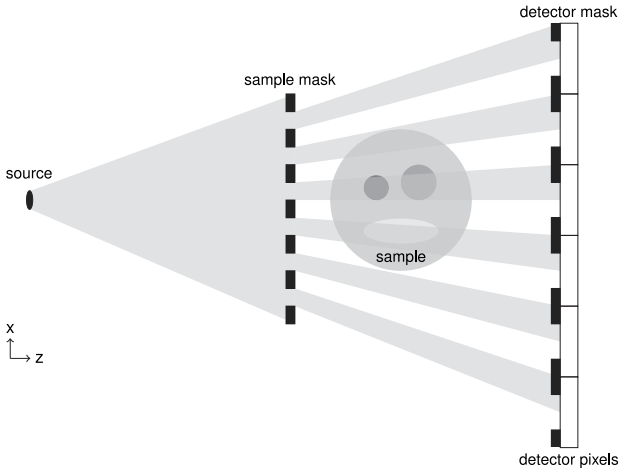

Fig. 10. Laboratory set-up for edge illumination X-ray phase-contrast imaging.

refraction [151]. This is typically achieved by recording two intensity projections, with the apertures aligned in such a way that the shaped X-ray beam impinges on the two edges of the detector aperture. If the apertures are aligned such that half of the intensity reaches the detector in both cases, these two configurations correspond to the two points at the full width half maximum of the illumination function (see Fig. 9b). The edge illumination principle can also be implemented with a laboratory set-up that uses rotating anode X-ray tubes with extended focal spots [152] (sketched in Fig. 10). The diverging and polychromatic beam generated by this type of sources is shaped by a pre-sample mask that creates a series of independent beamlets. These propagate through the sample and are then analysed by a second set of apertures before the detector. The pitches of both the pre-sample and the detector mask are harmonically matched to that of the detector pixels such that a one-to-one relationships exists between each aperture in both masks and each detector pixel column (along y). This approach has negligible spatial or temporal coherence requirements [153,154], provides high sensitivity also for laboratory implementations [155,156], enables the simultaneous attainment of high sensitivity and dynamic range [157], is robust against thermal and mechanical instabilities [158,159] and the set-up can be made compact [160,161]. By using a microfocal source it is possible to adopt a large magnification geometry and perform hard X-ray phase imaging with micrometre resolution [162]. Two-dimensional sensitivity can be simultaneously achieved by using masks structured in two dimensions [163].

Dark-field images can be quantitatively retrieved by acquiring (at least) a third intensity projection [164,165] and by using a Gaussian representation of the intensity. Under general conditions, the illumination function $L(\bar{x})$ (see Fig. 9b) can be expressed in the following way

$$I(\bar{x}) = \sum_m \sum_n A_{mn} \exp\left[-\frac{(\bar{x}-\mu_{mn})^2}{2\sigma_{mn}^2}\right] \tag{23}$$

where $\mu_{mn} = \mu_m + \mu_n$, $\sigma_{mn}^2 = \sigma_m^2 + \sigma_n^2$ and $A_{mn} = A_m A_n (1/\sqrt{2\pi\sigma_{mn}^2})$. Both the illumination function $L(\bar{x}) = \sum_n (A_n/\sqrt{2\pi\sigma_n^2}) \exp[-(\bar{x}-\mu_n)^2/2\sigma_n^2]$ and the object function $O(\bar{x}) = \sum_m (A_m/\sqrt{2\pi\sigma_m^2}) \exp[-(\bar{x}-\mu_m)^2/2\sigma_m^2]$ have been represented as the sum of Gaussian functions, ($m = 1 \dots M$ and $n = 1 \dots N$). A single-Gaussian representation of both illumination and object function is accurate in many practical cases and this allows for an analytic solution of Eq. (23) [164]. Should this not be the case, the number of terms to be retained in Eq. (23) can be increased and the sample's parameters retrieved numerically [159,166].

Tomographic edge-illumination X-ray phase-contrast imaging was developed at synchrotron sources [167] and adapted to rotating anode tubes [168,169], including three-dimensional dark-field imaging [157]. A reverse-projection reconstruction method enabled a step change in the data acquisition strategy by allowing continuous rotation of the sample [170,171]. More recent developments include algorithms for robust reconstructions [172,173] and a single-image phase retrieval algorithm [174] that, albeit requiring homogeneity of the sample, greatly simplifies the practical implementation of the method especially with respect to tomography [175]. This can be extended to include multi-material samples [176].

Examples of use in applied investigations of edge illumination X-ray phase contrast imaging are: low-dose mammography [177,178], cartilage imaging [179,180], security [181], baggage screening [182] with a large field of view scanning system [183–185], composites materials [186,187], regenerative medicine [188] and lung imaging [189].

5. Conclusion

X-ray phase-contrast imaging can extend the applicability of radiography and tomography for visualising the internal structure of samples that do not exhibit enough absorption contrast. Various methods have been developed to obtain phase contrast images in the hard X-ray regime, and they were introduced and described along with examples of applications. The edge illumination approach, that has been subject of investigation and developments by our group in the recent years, was finally presented and discussed.

Acknowledgements

ME was supported by the Royal Academy of Engineering under the RAEng Research Fellowships scheme. Fruitful discussion with the members of the Advanced X-ray Imaging Group at UCL is kindly acknowledged.

References

[1] W. Röntgen, Über eine neue art von strahlen: vorläufige mitteilung sitzungsber, Phys. Med. Gesell (1895).
[2] G.N. Hounsfield, Computerized transverse axial scanning (tomography): Part 1. Description of system, Br. J. Radiol. 46 (552) (1973) 1016–1022.
[3] S. Wilkins, Y.I. Nesterets, T. Gureyev, S. Mayo, A. Pogany, A. Stevenson, On the evolution and relative merits of hard X-ray phase-contrast imaging methods, Phil. Trans. R. Soc. A 372 (2010) (2014) 20130021.
[4] A. Olivo, E. Castelli, X-ray phase contrast imaging: From synchrotrons to conventional sources, Riv. Nuovo Cimento 37 (9) (2014) 467–508.
[5] P. Suortti, W. Thomlinson, Medical applications of synchrotron radiation, Phys. Med. Biol. 48 (13) (2003) R1.
[6] R. Lewis, Medical phase contrast X-ray imaging: current status and future prospects, Phys. Med. Biol. 49 (16) (2004) 3573.
[7] S.-A. Zhou, A. Brahme, Development of phase-contrast X-ray imaging techniques and potential medical applications, Phys. Med. 24 (3) (2008) 129–148.
[8] A. Bravin, P. Coan, P. Suortti, X-ray phase-contrast imaging: from pre-clinical applications towards clinics, Phys. Med. Biol. 58 (1) (2012) R1.
[9] P. Coan, A. Bravin, G. Tromba, Phase-contrast X-ray imaging of the breast: recent developments towards clinics, J. Phys. D: Appl. Phys. 46 (49) (2013) 494007.
[10] A. Stevenson, T. Gureyev, D. Paganin, S. Wilkins, T. Weitkamp, A. Snigirev, C. Rau, I. Snigireva, H. Youn, I. Dolbnya, et al., Phase-contrast X-ray imaging with synchrotron radiation for materials science applications, Nucl. Instrum. Methods Phys. Res. B 199 (2003) 427–435.
[11] S.C. Mayo, A.W. Stevenson, S.W. Wilkins, In-line phase-contrast X-ray imaging and tomography for materials science, Materials 5 (5) (2012) 937–965.
[12] T.E. Gureyev, Y. Nesterets, D. Ternovski, D. Thompson, S.W. Wilkins, A.W. Stevenson, A. Sakellariou, J.A. Taylor, Toolbox for advanced X-ray image processing, in: Proc Spie, Vol. 8141, 2011, pp. 81410B–14.
[13] M. Born, E. Wolf, Principles of Optics: Electromagnetic Theory of Propagation, Interference and Diffraction of Light, Elsevier, 1980.
[14] M. Endrizzi, P. Oliva, B. Golosio, P. Delogu, CMOS APS detector characterization for quantitative X-ray imaging, Nucl. Instrum. Methods Phys. Res., Sect. A 703 (2013) 26–32.
[15] D. Paganin, Coherent X-ray Optics, Oxford University Press on Demand, 2006.
[16] R. James, The Optical Principles of the Diffraction of X-rays, Bell and Sons, 1962.
[17] ICRU Tissue Substitutes in Radiation Dosimetry and Measurement, Report 44 of the International Commission on Radiation Units and Measurements, Bethesda, MD, 1989.

[18] U. Bonse, M. Hart, An X-ray interferometer, Appl. Phys. Lett. 6 (8) (1965) 155–156.
[19] U. Bonse, M. Hart, An X-ray interferometer with long separated interfering beam paths, Appl. Phys. Lett. 7 (4) (1965) 99–100.
[20] M. Hart, U. Bonse, Interferometry with x rays, Phys. Today 23 (8) (1970) 26–31.
[21] J.H. Bruning, D.R. Herriott, J. Gallagher, D. Rosenfeld, A. White, D. Brangaccio, Digital wavefront measuring interferometer for testing optical surfaces and lenses, Appl. Opt. 13 (11) (1974) 2693–2703.
[22] M. Ando, S. Hosoya, An attempt at X-ray phase-contrast microscopy, in: Proceedings of the 6th International Conference on X-Ray Optics and Microanalysis, University of Tokyo Press, Tokyo, 1972, pp. 63–68.
[23] M. Hart, Review lecture: Ten years of X-ray interferometry, Proc. R. Soc. A 346 (1644) (1975) 1–22.
[24] A. Momose, Demonstration of phase-contrast X-ray computed tomography using an X-ray interferometer, Nucl. Instrum. Methods Phys. Res., Sect. A 352 (3) (1995) 622–628.
[25] T. Takeda, A. Momose, Y. Itai, W. Jin, K. Hirano, Phase-contrast imaging with synchrotron X-rays for detecting cancer lesions, Acad. Radiol. 2 (9) (1995) 799–803.
[26] A. Momose, T. Takeda, Y. Itai, Phase-contrast X-ray computed tomography for observing biological specimens and organic materials, Rev. Sci. Instrum. 66 (2) (1995) 1434–1436.
[27] A. Momose, T. Takeda, Y. Itai, K. Hirano, Phase–contrast X–ray computed tomography for observing biological soft tissues, Nat. Med. 2 (4) (1996) 473–475.
[28] T. Takeda, A. Momose, E. Ueno, Y. Itai, Phase-contrast X-ray CT image of breast tumor, J. Synchrotron Radiat. 5 (3) (1998) 1133–1135.
[29] A. Momose, J. Fukuda, Phase-contrast radiographs of nonstained rat cerebellar specimen, Med. Phys. 22 (4) (1995) 375–379.
[30] A. Momose, T. Takeda, Y. Itai, Contrast effect of blood on phase-contrast X-ray imaging, Acad. Radiol. 2 (10) (1995) 883–887.
[31] A. Snigirev, I. Snigireva, V. Kohn, S. Kuznetsov, I. Schelokov, On the possibilities of X-ray phase contrast microimaging by coherent high-energy synchrotron radiation, Rev. Sci. Instrum. 66 (12) (1995) 5486–5492.
[32] P. Cloetens, R. Barrett, J. Baruchel, J.-P. Guigay, M. Schlenker, Phase objects in synchrotron radiation hard X-ray imaging, J. Phys. D: Appl. Phys. 29 (1) (1996) 133.
[33] S. Wilkins, T.E. Gureyev, D. Gao, A. Pogany, A. Stevenson, Phase-contrast imaging using polychromatic hard X-rays, Nature 384 (6607) (1996) 335.
[34] K.A. Nugent, Coherent methods in the X-ray sciences, Adv. Phys. 59 (1) (2010) 1–99.
[35] A. Pogany, D. Gao, S. Wilkins, Contrast and resolution in imaging with a microfocus X-ray source, Rev. Sci. Instrum. 68 (7) (1997) 2774–2782.
[36] Y.I. Nesterets, S. Wilkins, T. Gureyev, A. Pogany, A. Stevenson, On the optimization of experimental parameters for X-ray in-line phase-contrast imaging, Rev. Sci. Instrum. 76 (9) (2005) 093706.
[37] T.E. Gureyev, Y.I. Nesterets, A.W. Stevenson, P.R. Miller, A. Pogany, S.W. Wilkins, Some simple rules for contrast, signal-to-noise and resolution in in-line X-ray phase-contrast imaging, Opt. Express 16 (5) (2008) 3223–3241.
[38] K. Nugent, T. Gureyev, D. Cookson, D. Paganin, Z. Barnea, Quantitative phase imaging using hard x rays, Phys. Rev. Lett. 77 (14) (1996) 2961.
[39] T. Gureyev, S. Wilkins, On X-ray phase imaging with a point source, J. Opt. Soc. Amer. A 15 (3) (1998) 579–585.
[40] T. Gureyev, C. Raven, A. Snigirev, I. Snigireva, S. Wilkins, Hard X-ray quantitative non-interferometric phase-contrast microscopy, J. Phys. D: Appl. Phys. 32 (5) (1999) 563.
[41] T.E. Gureyev, C. Raven, A.A. Snigirev, I. Snigireva, S.W. Wilkins, Hard X-ray quantitative noninterferometric phase-contrast imaging, in: Medical Imaging'99, International Society for Optics and Photonics, 1999, pp. 356–364.
[42] T. Gureyev, S. Wilkins, On X-ray phase retrieval from polychromatic images, Opt. Commun. 147 (4) (1998) 229–232.
[43] T. Gureyev, S. Mayo, S. Wilkins, D. Paganin, A. Stevenson, Quantitative in-line phase-contrast imaging with multienergy x rays, Phys. Rev. Lett. 86 (25) (2001) 5827.
[44] P. Cloetens, W. Ludwig, J. Baruchel, D. Van Dyck, J. Van Landuyt, J. Guigay, M. Schlenker, Holotomography: Quantitative phase tomography with micrometer resolution using hard synchrotron radiation x rays, Appl. Phys. Lett. 75 (19) (1999) 2912–2914.
[45] A.V. Bronnikov, Reconstruction formulas in phase-contrast tomography, Opt. Commun. 171 (4) (1999) 239–244.
[46] A. Barty, K. Nugent, A. Roberts, D. Paganin, Quantitative phase tomography, Opt. Commun. 175 (4) (2000) 329–336.
[47] D. Paganin, S. Mayo, T.E. Gureyev, P.R. Miller, S.W. Wilkins, Simultaneous phase and amplitude extraction from a single defocused image of a homogeneous object, J. Microsc. 206 (1) (2002) 33–40.
[48] P. Cloetens, M. Pateyron-Salomé, J. Buffiere, G. Peix, J. Baruchel, F. Peyrin, M. Schlenker, Observation of microstructure and damage in materials by phase sensitive radiography and tomography, J. Appl. Phys. 81 (9) (1997) 5878–5886.
[49] J.-Y. Buffière, E. Maire, P. Cloetens, G. Lormand, R. Fougeres, Characterization of internal damage in a MMC p using X-ray synchrotron phase contrast microtomography, Acta Mater. 47 (5) (1999) 1613–1625.
[50] P. Spanne, C. Raven, I. Snigireva, A. Snigirev, In-line holography and phase-contrast microtomography with high energy X-rays, Phys. Med. Biol. 44 (3) (1999) 741.
[51] P. Bleuet, P. Cloetens, P. Gergaud, D. Mariolle, N. Chevalier, R. Tucoulou, J. Susini, A. Chabli, A hard X-ray nanoprobe for scanning and projection nanotomography, Rev. Sci. Instrum. 80 (5) (2009) 056101.
[52] M. Langer, A. Pacureanu, H. Suhonen, Q. Grimal, P. Cloetens, F. Peyrin, X-ray phase nanotomography resolves the 3D human bone ultrastructure, PLoS One 7 (8) (2012) e35691.
[53] H. Suhonen, F. Xu, L. Helfen, C. Ferrero, P. Vladimirov, P. Cloetens, X-ray phase contrast and fluorescence nanotomography for material studies, Int. J. Mater. Res. 103 (2) (2012) 179–183.
[54] P. Varga, A. Pacureanu, M. Langer, H. Suhonen, B. Hesse, Q. Grimal, P. Cloetens, K. Raum, F. Peyrin, Investigation of the three-dimensional orientation of mineralized collagen fibrils in human lamellar bone using synchrotron X-ray phase nanotomography, Acta Biomater. 9 (9) (2013) 8118–8127.
[55] M. Kitchen, D. Paganin, R. Lewis, N. Yagi, K. Uesugi, S. Mudie, On the origin of speckle in X-ray phase contrast images of lung tissue, Phys. Med. Biol. 49 (18) (2004) 4335.
[56] S.B. Hooper, M.J. Kitchen, M.J. Wallace, N. Yagi, K. Uesugi, M.J. Morgan, C. Hall, K.K. Siu, I.M. Williams, M. Siew, et al., Imaging lung aeration and lung liquid clearance at birth, FASEB J. 21 (12) (2007) 3329–3337.
[57] M. Kitchen, R. Lewis, M. Morgan, M. Wallace, M. Siew, K. Siu, A. Habib, A. Fouras, N. Yagi, K. Uesugi, et al., Dynamic measures of regional lung air volume using phase contrast X-ray imaging, Phys. Med. Biol. 53 (21) (2008) 6065.
[58] M. Kitchen, R. Lewis, N. Yagi, K. Uesugi, D. Paganin, S. Hooper, G. Adams, S. Jureczek, J. Singh, C. Christensen, et al., Phase contrast X-ray imaging of mice and rabbit lungs: a comparative study, Br. J. Radiol. (2014).
[59] R.P. Murrie, K.S. Morgan, A. Maksimenko, A. Fouras, D.M. Paganin, C. Hall, K.K. Siu, D.W. Parsons, M. Donnelley, Live small-animal X-ray lung velocimetry and lung micro-tomography at the Australian synchrotron imaging and medical beamline, J. Synchrotron Radiat. 22 (4) (2015) 1049–1055.
[60] M. Di Michiel, A. Olivo, G. Tromba, F. Arfelli, V. Bonvicini, A. Bravin, G. Cantatore, E. Castelli, L.D. Palma, R. Longo, S. Pani, D. Pontoni, P. Poropat, M. Prest, A. Rashevsky, A. Vacchi, E. Vallazza, Phase contrast imaging in the field of mammography, in: M. Ando, C. Uyama (Eds.), Medical Applications of Synchrotron Radiation, 1998, pp. 78–82.
[61] F. Arfelli, M. Assante, V. Bonvicini, A. Bravin, G. Cantatore, E. Castelli, L.D. Palma, M.D. Michiel, R. Longo, A. Olivo, S. Pani, D. Pontoni, P. Poropat, M. Prest, A. Rashevsky, G. Tromba, A. Vacchi, E. Vallazza, F. Zanconati, Low-dose phase contrast X-ray medical imaging, Phys. Med. Biol. 43 (10) (1998) 2845.
[62] E. Castelli, F. Arfelli, D. Dreossi, R. Longo, T. Rokvic, M. Cova, E. Quaia, M. Tonutti, F. Zanconati, A. Abrami, et al., Clinical mammography at the syrmep beam line, Nucl. Instrum. Methods Phys. Res., Sect. A 572 (1) (2007) 237–240.
[63] E. Castelli, M. Tonutti, F. Arfelli, R. Longo, E. Quaia, L. Rigon, D. Sanabor, F. Zanconati, D. Dreossi, A. Abrami, et al., Mammography with synchrotron radiation: first clinical experience with phase-detection technique, Radiology 259 (3) (2011) 684–694.
[64] R. Longo, M. Tonutti, L. Rigon, F. Arfelli, D. Dreossi, E. Quai, F. Zanconati, E. Castelli, G. Tromba, M.A. Cova, Clinical study in phase-contrast mammography: image-quality analysis, Phil. Trans. R. Soc. A 372 (2010) (2014) 20130025.
[65] F. Arfelli, V. Bonvicini, A. Bravin, G. Cantatore, E. Castelli, L.D. Palma, M.D. Michiel, M. Fabrizioli, R. Longo, R.H. Menk, et al., Mammography with synchrotron radiation: Phase-detection techniques 1, Radiology 215 (1) (2000) 286–293.
[66] K. Goetz, M. Kalashnikov, Y.A. Mikhailov, G.V. Sklizkov, S. Fedotov, E. Foerster, P. Zaumseil, Measurements of the parameters of shell targets for laser thermonuclear fusion using an X-ray schlieren method, Sov. J. Quantum Electron. 9 (5) (1979) 607.
[67] E. Forster, K. Goetz, P. Zaumseil, Double crystal diffractometry for the characterization of targets for laser fusion experiments, Krist. Tech. 15 (8) (1980) 937–945.
[68] T. Davis, D. Gao, T. Gureyev, A. Stevenson, S. Wilkins, et al., Phase-contrast imaging of weakly absorbing materials using hard X-rays, Nature 373 (6515) (1995) 595–598.
[69] V. Ingal, E. Beliaevskaya, X-ray plane-wave topography observation of the phase contrast from a non-crystalline object, J. Phys. D: Appl. Phys. 28 (11) (1995) 2314.
[70] D. Chapman, W. Thomlinson, R. Johnston, D. Washburn, E. Pisano, N. Gmür, Z. Zhong, R. Menk, F. Arfelli, D. Sayers, Diffraction enhanced X-ray imaging, Phys. Med. Biol. 42 (11) (1997) 2015.
[71] F. Dilmanian, Z. Zhong, B. Ren, X. Wu, L. Chapman, I. Orion, W. Thomlinson, Computed tomography of X-ray index of refraction using the diffraction enhanced imaging method, Phys. Med. Biol. 45 (4) (2000) 933.
[72] Y.I. Nesterets, T. Gureyev, D. Paganin, K. Pavlov, S. Wilkins, Quantitative diffraction-enhanced X-ray imaging of weak objects, J. Phys. D: Appl. Phys. 37 (8) (2004) 1262.
[73] T. Gureyev, S. Wilkins, Regimes of X-ray phase-contrast imaging with perfect crystals, Nuovo Cimento D 19 (2) (1997) 545–552.
[74] M.N. Wernick, O. Wirjadi, D. Chapman, Z. Zhong, N.P. Galatsanos, Y. Yang, J.G. Brankov, O. Oltulu, M.A. Anastasio, C. Muehleman, Multiple-image radiography, Phys. Med. Biol. 48 (23) (2003) 3875.

[75] O. Oltulu, Z. Zhong, M. Hasnah, M.N. Wernick, D. Chapman, Extraction of extinction, refraction and absorption properties in diffraction enhanced imaging, J. Phys. D: Appl. Phys. 36 (17) (2003) 2152.
[76] L. Rigon, H.-J. Besch, F. Arfelli, R.-H. Menk, G. Heitner, H. Plothow-Besch, A new DEI algorithm capable of investigating sub-pixel structures, J. Phys. D: Appl. Phys. 36 (10A) (2003) A107.
[77] E. Pagot, P. Cloetens, S. Fiedler, A. Bravin, P. Coan, J. Baruchel, J. Härtwig, W. Thomlinson, A method to extract quantitative information in analyzer-based X-ray phase contrast imaging, Appl. Phys. Lett. 82 (20) (2003) 3421–3423.
[78] L. Rigon, A. Astolfo, F. Arfelli, R.-H. Menk, Generalized diffraction enhanced imaging: application to tomography, Eur. J. Radiol. 68 (3) (2008) S3–S7.
[79] M.J. Kitchen, D.M. Paganin, K. Uesugi, B.J. Allison, R.A. Lewis, S.B. Hooper, K.M. Pavlov, X-ray phase, absorption and scatter retrieval using two or more phase contrast images, Opt. Express 18 (19) (2010) 19994–20012.
[80] D. Chapman, E. Pisano, W. Thomlinson, Z. Zhong, R. Johnston, D. Washburn, D. Sayers, K. Malinowska, Medical applications of diffraction enhanced imaging, Breast Dis. 10 (3–4) (1998) 197–207.
[81] J. Mollenhauer, M. Aurich, Z. Zhong, C. Muehleman, A. Cole, M. Hasnah, O. Oltulu, K. Kuettner, A. Margulis, L. Chapman, Diffraction-enhanced X-ray imaging of articular cartilage, Osteoarthritis Cartilage 10 (3) (2002) 163–171.
[82] P. Coan, F. Bamberg, P.C. Diemoz, A. Bravin, K. Timpert, E. Mützel, J.G. Raya, S. Adam-Neumair, M.F. Reiser, C. Glaser, Characterization of osteoarthritic and normal human patella cartilage by computed tomography X-ray phase-contrast imaging: a feasibility study, Invest. Radiol. 45 (7) (2010) 437–444.
[83] P. Coan, A. Wagner, A. Bravin, P.C. Diemoz, J. Keyriläinen, J. Mollenhauer, In vivo X-ray phase contrast analyzer-based imaging for longitudinal osteoarthritis studies in guinea pigs, Phys. Med. Biol. 55 (24) (2010) 7649.
[84] C. Muehleman, J. Li, D. Connor, C. Parham, E. Pisano, Z. Zhong, Diffraction-enhanced imaging of musculoskeletal tissues using a conventional X-ray tube, Acad. Radiol. 16 (8) (2009) 918–923.
[85] V.N. Ingal, E.A. Beliaevskaya, A.P. Brianskaya, R.D. Merkurieva, Phase mammography-a new technique for breast investigation, Phys. Med. Biol. 43 (9) (1998) 2555.
[86] E.D. Pisano, R.E. Johnston, D. Chapman, J. Geradts, M.V. Iacocca, C.A. Livasy, D.B. Washburn, D.E. Sayers, Z. Zhong, M.Z. Kiss, et al., Human breast cancer specimens: Diffraction-enhanced imaging with histologic correlation?improved conspicuity of lesion detail compared with digital radiography 1, Radiology 214 (3) (2000) 895–901.
[87] A. Sztrókay, P. Diemoz, T. Schlossbauer, E. Brun, F. Bamberg, D. Mayr, M. Reiser, A. Bravin, P. Coan, High-resolution breast tomography at high energy: a feasibility study of phase contrast imaging on a whole breast, Phys. Med. Biol. 57 (10) (2012) 2931.
[88] T. Millard, M. Endrizzi, L. Rigon, F. Arfelli, R. Menk, J. Owen, E. Stride, A. Olivo, Quantification of microbubble concentration through X-ray phase contrast imaging, Appl. Phys. Lett. 103 (11) (2013) 114105.
[89] T. Millard, M. Endrizzi, N. Everdell, L. Rigon, F. Arfelli, R. Menk, E. Stride, A. Olivo, Evaluation of microbubble contrast agents for dynamic imaging with X-ray phase contrast, Sci. Rep. 5 (2015).
[90] F. Pfeiffer, A. Momose, W. Yashiro, Milestones and basic principles of grating-based X-ray and neutron phase-contrast imaging, AIP Conf. Proc. 1466 (1) (2012) 2–11.
[91] J. Clauser, M. Reinsch, New theoretical and experimental results in Fresnel optics with applications to matter-wave and X-ray interferometry, Appl. Phys. B: Lasers Opt. 54 (5) (1992) 380–395.
[92] J.F. Clauser, Ultrahigh resolution interferometric X-ray imaging, US Patent 5,812,629, 1998.
[93] P. Cloetens, J. Guigay, C. De Martino, J. Baruchel, M. Schlenker, Fractional Talbot imaging of phase gratings with hard x rays, Opt. Lett. 22 (14) (1997) 1059–1061.
[94] P. Cloetens, J.-P. Guigay, C. De Martino, M. Pateyron-Salome, M. Schlenker, D. Van Dyck, Quantitative aspects of coherent hard X-ray imaging: Talbot images and holographic reconstruction, in: Optical Science, Engineering and Instrumentation'97, International Society for Optics and Photonics, 1997, pp. 72–82.
[95] C. David, B. Nöhammer, H. Solak, E. Ziegler, Differential X-ray phase contrast imaging using a shearing interferometer, Appl. Phys. Lett. 81 (17) (2002) 3287–3289.
[96] A. Momose, S. Kawamoto, I. Koyama, Y. Hamaishi, K. Takai, Y. Suzuki, Demonstration of X-ray Talbot interferometry, Japan. J. Appl. Phys. 42 (7B) (2003) L866.
[97] T. Weitkamp, A. Diaz, C. David, F. Pfeiffer, M. Stampanoni, P. Cloetens, E. Ziegler, X-ray phase imaging with a grating interferometer, Opt. Express 13 (16) (2005) 6296–6304.
[98] F. Pfeiffer, T. Weitkamp, O. Bunk, C. David, Phase retrieval and differential phase-contrast imaging with low-brilliance X-ray sources, Nat. Phys. 2 (4) (2006) 258–261.
[99] F. Pfeiffer, C. Kottler, O. Bunk, C. David, Hard X-ray phase tomography with low-brilliance sources, Phys. Rev. Lett. 98 (10) (2007) 108105.
[100] F. Pfeiffer, M. Bech, O. Bunk, P. Kraft, E.F. Eikenberry, C. Brönnimann, C. Grünzweig, C. David, Hard-X-ray dark-field imaging using a grating interferometer, Nature Mater. 7 (2) (2008) 134–137.
[101] Z.-F. Huang, K.-J. Kang, L. Zhang, Z.-Q. Chen, F. Ding, Z.-T. Wang, Q.-G. Fang, Alternative method for differential phase-contrast imaging with weakly coherent hard x rays, Phys. Rev. A 79 (1) (2009) 013815.
[102] Z.-T. Wang, K.-J. Kang, Z.-F. Huang, Z.-Q. Chen, Quantitative grating-based X-ray dark-field computed tomography, Appl. Phys. Lett. 95 (9) (2009) 094105.
[103] M. Bech, O. Bunk, T. Donath, R. Feidenhans, C. David, F. Pfeiffer, Quantitative X-ray dark-field computed tomography, Phys. Med. Biol. 55 (18) (2010) 5529.
[104] I. Zanette, T. Weitkamp, T. Donath, S. Rutishauser, C. David, Two-dimensional X-ray grating interferometer, Phys. Rev. Lett. 105 (24) (2010) 248102.
[105] H. Itoh, K. Nagai, G. Sato, K. Yamaguchi, T. Nakamura, T. Kondoh, C. Ouchi, T. Teshima, Y. Setomoto, T. Den, Two-dimensional grating-based X-ray phase-contrast imaging using Fourier transform phase retrieval, Opt. Express 19 (4) (2011) 3339–3346.
[106] G. Sato, T. Kondoh, H. Itoh, S. Handa, K. Yamaguchi, T. Nakamura, K. Nagai, C. Ouchi, T. Teshima, Y. Setomoto, et al., Two-dimensional gratings-based phase-contrast imaging using a conventional X-ray tube, Opt. Lett. 36 (18) (2011) 3551–3553.
[107] B. Wu, Y. Liu, C. Rose-Petruck, G.J. Diebold, X-ray spatial frequency heterodyne imaging, Appl. Phys. Lett. 100 (6) (2012) 061110.
[108] T. Donath, M. Chabior, F. Pfeiffer, O. Bunk, E. Reznikova, J. Mohr, E. Hempel, S. Popescu, M. Hoheisel, M. Schuster, et al., Inverse geometry for grating-based X-ray phase-contrast imaging, J. Appl. Phys. 106 (5) (2009) 054703.
[109] N. Morimoto, S. Fujino, K.-i. Ohshima, J. Harada, T. Hosoi, H. Watanabe, T. Shimura, X-ray phase contrast imaging by compact Talbot–Lau interferometer with a single transmission grating, Opt. Lett. 39 (15) (2014) 4297–4300.
[110] H. Miao, A.A. Gomella, N. Chedid, L. Chen, H. Wen, Fabrication of 200 nm period hard X-ray phase gratings, Nano Lett. 14 (6) (2014) 3453.
[111] H. Miao, A.A. Gomella, K.J. Harmon, E.E. Bennett, N. Chedid, S. Znati, A. Panna, B.A. Foster, P. Bhandarkar, H. Wen, Enhancing tabletop X-ray phase contrast imaging with nano-fabrication, Sci. Rep. 5 (2015).
[112] H. Miao, A. Panna, A.A. Gomella, E.E. Bennett, S. Znati, L. Chen, H. Wen, A universal moiré effect and application in X-ray phase-contrast imaging, Nat. Phys. 12 (9) (2016) 830–834.
[113] Z. Wang, N. Hauser, G. Singer, M. Trippel, R.A. Kubik-Huch, C.W. Schneider, M. Stampanoni, Non-invasive classification of microcalcifications with phase-contrast X-ray mammography, Nature Commun. 5 (2014).
[114] T. Michel, J. Rieger, G. Anton, F. Bayer, M.W. Beckmann, J. Durst, P.A. Fasching, W. Haas, A. Hartmann, G. Pelzer, et al., On a dark-field signal generated by micrometer-sized calcifications in phase-contrast mammography, Phys. Med. Biol. 58 (8) (2013) 2713.
[115] M. Stampanoni, Z. Wang, T. Thüring, C. David, E. Roessl, M. Trippel, R.A. Kubik-Huch, G. Singer, M.K. Hohl, N. Hauser, The first analysis and clinical evaluation of native breast tissue using differential phase-contrast mammography, Invest. Radiol. 46 (12) (2011) 801–806.
[116] F. Pfeiffer, O. Bunk, C. David, M. Bech, G. Le Duc, A. Bravin, P. Cloetens, High-resolution brain tumor visualization using three-dimensional X-ray phase contrast tomography, Phys. Med. Biol. 52 (23) (2007) 6923.
[117] A. Momose, W. Yashiro, K. Kido, J. Kiyohara, C. Makifuchi, T. Ito, S. Nagatsuka, C. Honda, D. Noda, T. Hattori, et al., X-ray phase imaging: from synchrotron to hospital, Phil. Trans. R. Soc. A 372 (2010) (2014) 20130023.
[118] J. Tanaka, M. Nagashima, K. Kido, Y. Hoshino, J. Kiyohara, C. Makifuchi, S. Nishino, S. Nagatsuka, A. Momose, Cadaveric and in vivo human joint imaging based on differential phase contrast by X-ray Talbot-Lau interferometry, Z. Med. Phys. 23 (3) (2013) 222–227.
[119] D. Stutman, T.J. Beck, J.A. Carrino, C.O. Bingham, Talbot phase-contrast X-ray imaging for the small joints of the hand, Phys. Med. Biol. 56 (17) (2011) 5697.
[120] T. Thüring, R. Guggenberger, H. Alkadhi, J. Hodler, M. Vich, Z. Wang, C. David, M. Stampanoni, Human hand radiography using X-ray differential phase contrast combined with dark-field imaging, Skeletal Radiol. 42 (6) (2013) 827–835.
[121] S. Schleede, F.G. Meinel, M. Bech, J. Herzen, K. Achterhold, G. Potdevin, A. Malecki, S. Adam-Neumair, S.F. Thieme, F. Bamberg, et al., Emphysema diagnosis using X-ray dark-field imaging at a laser-driven compact synchrotron light source, Proc. Natl. Acad. Sci. 109 (44) (2012) 17880–17885.
[122] M. Bech, A. Tapfer, A. Velroyen, A. Yaroshenko, B. Pauwels, J. Hostens, P. Bruyndonckx, A. Sasov, F. Pfeiffer, In-vivo dark-field and phase-contrast X-ray imaging, Sci. Rep. 3 (2013) 3209.
[123] F. Pfeiffer, J. Herzen, M. Willner, M. Chabior, S. Auweter, M. Reiser, F. Bamberg, Grating-based X-ray phase contrast for biomedical imaging applications, Z. Med. Phys. 23 (3) (2013) 176–185.
[124] S. Wilkins, Improved X-ray optics, especially for phase-contrast imaging, International Patent WO 1995005725, 1995, A1.
[125] S. Wilkins, On a spatially resolving USAXS instrument for operation at a third-generation synchrotron radiation source, J. Synchrotron Radiat. 5 (3) (1998) 986–988.
[126] S.C. Mayo, B. Sexton, Refractive microlens array for wave-front analysis in the medium to hard X-ray range, Opt. Lett. 29 (8) (2004) 866–868.
[127] M. De Jonge, B. Hornberger, C. Holzner, D. Legnini, D. Paterson, I. McNulty, C. Jacobsen, S. Vogt, Quantitative phase imaging with a scanning transmission X-ray microscope, Phys. Rev. Lett. 100 (16) (2008) 163902.

[128] K.S. Morgan, D.M. Paganin, K.K. Siu, Quantitative single-exposure X-ray phase contrast imaging using a single attenuation grid, Opt. Express 19 (20) (2011) 19781–19789.
[129] F.A. Vittoria, M. Endrizzi, P.C. Diemoz, U.H. Wagner, C. Rau, I.K. Robinson, A. Olivo, Virtual edge illumination and one dimensional beam tracking for absorption, refraction, and scattering retrieval, Appl. Phys. Lett. 104 (13) (2014) 134102.
[130] F.A. Vittoria, G.K. Kallon, D. Basta, P.C. Diemoz, I.K. Robinson, A. Olivo, M. Endrizzi, Beam tracking approach for single–shot retrieval of absorption, refraction, and dark–field signals with laboratory x–ray sources, Appl. Phys. Lett. 106 (22) (2015) 224102.
[131] K.S. Morgan, D.M. Paganin, K.K. Siu, Quantitative X-ray phase-contrast imaging using a single grating of comparable pitch to sample feature size, Opt. Lett. 36 (1) (2011) 55–57.
[132] R. Cerbino, L. Peverini, M. Potenza, A. Robert, P. Bösecke, M. Giglio, X-ray-scattering information obtained from near-field speckle, Nat. Phys. 4 (3) (2008) 238–243.
[133] K.S. Morgan, D.M. Paganin, K.K. Siu, X-ray phase imaging with a paper analyzer, Appl. Phys. Lett. 100 (12) (2012) 124102.
[134] F. Krejci, J. Jakubek, M. Kroupa, Hard X-ray phase contrast imaging using single absorption grating and hybrid semiconductor pixel detector, Rev. Sci. Instrum. 81 (11) (2010) 113702.
[135] H. Wen, E.E. Bennett, M.M. Hegedus, S.C. Carroll, Spatial harmonic imaging of X-ray scattering?initial results, IEEE Trans. Med. Imaging 27 (8) (2008) 997–1002.
[136] H.H. Wen, E.E. Bennett, R. Kopace, A.F. Stein, V. Pai, Single-shot X-ray differential phase-contrast and diffraction imaging using two-dimensional transmission gratings, Opt. Lett. 35 (12) (2010) 1932–1934.
[137] F. Krejci, J. Jakubek, M. Kroupa, Low dose X-ray phase contrast imaging sensitive to phase effects in 2-D, in: Nuclear Science Symposium Conference Record (NSS/MIC), 2010 IEEE, IEEE, 2010, pp. 2194–2199.
[138] S. Bérujon, E. Ziegler, R. Cerbino, L. Peverini, Two-dimensional X-ray beam phase sensing, Phys. Rev. Lett. 108 (15) (2012) 158102.
[139] S. Berujon, H. Wang, K. Sawhney, X-ray multimodal imaging using a random-phase object, Phys. Rev. A 86 (6) (2012) 063813.
[140] I. Zanette, T. Zhou, A. Burvall, U. Lundström, D.H. Larsson, M. Zdora, P. Thibault, F. Pfeiffer, H.M. Hertz, Speckle-based X-ray phase-contrast and dark-field imaging with a laboratory source, Phys. Rev. Lett. 112 (25) (2014) 253903.
[141] T.H. Jensen, M. Bech, O. Bunk, T. Donath, C. David, R. Feidenhans, F. Pfeiffer, Directional X-ray dark-field imaging, Phys. Med. Biol. 55 (12) (2010) 3317.
[142] H. Wang, S. Berujon, J. Herzen, R. Atwood, D. Laundy, A. Hipp, K. Sawhney, X-ray phase contrast tomography by tracking near field speckle, Sci. Rep. 5 (2015) 8762.
[143] M. Kagias, Z. Wang, P. Villanueva-Perez, K. Jefimovs, M. Stampanoni, 2D-Omnidirectional hard-X-ray scattering sensitivity in a single shot, Phys. Rev. Lett. 116 (9) (2016) 093902.
[144] F.A. Vittoria, M. Endrizzi, P.C. Diemoz, A. Zamir, U.H. Wagner, C. Rau, I.K. Robinson, A. Olivo, X–ray absorption, phase and dark–field tomography through a beam tracking approach, Sci. Rep. 5 (2015) 16318.
[145] H. Wen, E.E. Bennett, M.M. Hegedus, S. Rapacchi, Fourier X-ray scattering radiography yields bone structural information 1, Radiology 251 (3) (2009) 910–918.
[146] K.S. Morgan, M. Donnelley, D.M. Paganin, A. Fouras, N. Yagi, Y. Suzuki, A. Takeuchi, K. Uesugi, R.C. Boucher, D.W. Parsons, et al., Measuring airway surface liquid depth in ex vivo mouse airways by X-ray imaging for the assessment of cystic fibrosis airway therapies, PLoS One 8 (1) (2013) e55822.
[147] K.S. Morgan, M. Donnelley, N. Farrow, A. Fouras, N. Yagi, Y. Suzuki, A. Takeuchi, K. Uesugi, R.C. Boucher, K.K. Siu, et al., In vivo X-ray imaging reveals improved airway surface hydration after a therapy designed for cystic fibrosis, Amer. J. Respir. Crit. Care Med. 190 (4) (2014) 469–472.
[148] S. Berujon, H. Wang, S. Alcock, K. Sawhney, At-wavelength metrology of hard X-ray mirror using near field speckle, Opt. Express 22 (6) (2014) 6438–6446.
[149] S. Berujon, E. Ziegler, P. Cloetens, X-ray pulse wavefront metrology using speckle tracking, J. Synchrotron Radiat. 22 (4) (2015) 886–894.
[150] A. Olivo, F. Arfelli, G. Cantatore, R. Longo, R. Menk, S. Pani, M. Prest, P. Poropat, L. Rigon, G. Tromba, et al., An innovative digital imaging set-up allowing a low-dose approach to phase contrast applications in the medical field, Med. Phys. 28 (8) (2001) 1610–1619.
[151] P.R. Munro, K. Ignatyev, R.D. Speller, A. Olivo, Phase and absorption retrieval using incoherent X-ray sources, Proc. Natl. Acad. Sci. 109 (35) (2012) 13922–13927.
[152] A. Olivo, R. Speller, A coded-aperture technique allowing X-ray phase contrast imaging with conventional sources, Appl. Phys. Lett. 91 (7) (2007) 074106.
[153] P.R. Munro, K. Ignatyev, R.D. Speller, A. Olivo, Source size and temporal coherence requirements of coded aperture type X-ray phase contrast imaging systems., Opt. Express 18 (19) (2010) 19681–19692.
[154] M. Endrizzi, F.A. Vittoria, G. Kallon, D. Basta, P.C. Diemoz, A. Vincenzi, P. Delogu, R. Bellazzini, A. Olivo, Achromatic approach to phase-based multi-modal imaging with conventional X-ray sources, Opt. Express 23 (12) (2015) 16473–16480.
[155] P. Diemoz, M. Endrizzi, C. Zapata, Z. Pešić, C. Rau, A. Bravin, I. Robinson, A. Olivo, X-ray phase-contrast imaging with nanoradian angular resolution, Phys. Rev. Lett. 110 (13) (2013) 138105.
[156] P. Diemoz, C. Hagen, M. Endrizzi, A. Olivo, Sensitivity of laboratory based implementations of edge illumination X-ray phase-contrast imaging, Appl. Phys. Lett. 103 (24) (2013) 244104.
[157] M. Endrizzi, F. Vittoria, L. Rigon, D. Dreossi, F. Iacoviello, P. Shearing, A. Olivo, X-ray phase-contrast radiography and tomography with a multiaperture analyzer, Phys. Rev. Lett. 118 (24) (2017) 243902.
[158] T. Millard, M. Endrizzi, K. Ignatyev, C. Hagen, P. Munro, R. Speller, A. Olivo, Method for automatization of the alignment of a laboratory based X-ray phase contrast edge illumination system, Rev. Sci. Instrum. 84 (8) (2013) 083702.
[159] M. Endrizzi, D. Basta, A. Olivo, Laboratory-based X-ray phase-contrast imaging with misaligned optical elements, Appl. Phys. Lett. 107 (12) (2015) 124103.
[160] D. Basta, M. Endrizzi, F. Vittoria, G. Kallon, T. Millard, P. Diemoz, A. Olivo, Note: Design and realization of a portable edge illumination X-ray phase contrast imaging system, Rev. Sci. Instrum. 86 (9) (2015) 096102.
[161] D. Basta, M. Endrizzi, F. Vittoria, A. Astolfo, A. Olivo, Compact and cost effective lab-based edge-illumination X-ray phase contrast imaging with a structured focal spot, Appl. Phys. Lett. 108 (22) (2016) 224102.
[162] M. Endrizzi, F.A. Vittoria, P.C. Diemoz, R. Lorenzo, R.D. Speller, U.H. Wagner, C. Rau, I.K. Robinson, A. Olivo, Phase-contrast microscopy at high X-ray energy with a laboratory setup, Opt. Lett. 39 (11) (2014) 3332–3335.
[163] G.K. Kallon, M. Wesolowski, F.A. Vittoria, M. Endrizzi, D. Basta, T.P. Millard, P.C. Diemoz, A. Olivo, A laboratory based edge-illumination X-ray phase-contrast imaging setup with two-directional sensitivity, Appl. Phys. Lett. 107 (20) (2015) 204105.
[164] M. Endrizzi, P.C. Diemoz, T.P. Millard, J. Louise Jones, R.D. Speller, I.K. Robinson, A. Olivo, Hard X-ray dark-field imaging with incoherent sample illumination, Appl. Phys. Lett. 104 (2) (2014) 024106.
[165] M. Endrizzi, P.C. Diemoz, C.K. Hagen, T.P. Millard, F.A. Vittoria, U.H. Wagner, C. Rau, I.K. Robinson, A. Olivo, Laboratory-based edge-illumination phase-contrast imaging: Dark-field retrieval and high-resolution implementations, in: Nuclear Science Symposium and Medical Imaging Conference (NSS/MIC), 2014 IEEE, IEEE, 2014, pp. 1–4.
[166] A. Astolfo, M. Endrizzi, G. Kallon, T.P. Millard, F.A. Vittoria, A. Olivo, A first investigation of accuracy, precision and sensitivity of phase-based X-ray dark-field imaging, J. Phys. D: Appl. Phys. 49 (48) (2016) 485501.
[167] C. Hagen, P. Diemoz, M. Endrizzi, L. Rigon, D. Dreossi, F. Arfelli, F. Lopez, R. Longo, A. Olivo, Theory and preliminary experimental verification of quantitative edge illumination X-ray phase contrast tomography, Opt. Express 22 (7) (2014) 7989–8000.
[168] C. Hagen, P. Munro, M. Endrizzi, P. Diemoz, A. Olivo, Low-dose phase contrast tomography with conventional X-ray sources, Med. Phys. 41 (7) (2014).
[169] C.K. Hagen, A. Zamir, P.C. Diemoz, M. Endrizzi, F. Kennedy, R.H. Jager, A. Olivo, Low-dose X-ray phase contrast tomography: Experimental setup, image reconstruction and applications in biomedicine, in: Nuclear Science Symposium and Medical Imaging Conference (NSS/MIC), 2014 IEEE, IEEE, 2014, pp. 1–5.
[170] C.K. Hagen, M. Endrizzi, P.C. Diemoz, A. Olivo, Reverse projection retrieval in edge illumination X-ray phase contrast computed tomography, J. Phys. D: Appl. Phys. 49 (25) (2016) 255501.
[171] C.K. Hagen, P. Maghsoudlou, G. Totonelli, P.C. Diemoz, M. Endrizzi, A. Zamir, P. Coan, A. Bravin, P. De Coppi, A. Olivo, Strategies for fast and low-dose laboratory-based phase contrast tomography for microstructural scaffold analysis in tissue engineering, in: SPIE Optical Engineering + Applications, International Society for Optics and Photonics, 2016, pp. 996705-1–996705-7.
[172] A. Zamir, M. Endrizzi, C.K. Hagen, F.A. Vittoria, L. Urbani, P. De Coppi, A. Olivo, Robust phase retrieval for high resolution edge illumination X-ray phase-contrast computed tomography in non-ideal environments, Sci. Rep. 6 (2016).
[173] A. Zamir, C.K. Hagen, P.C. Diemoz, M. Endrizzi, F.A. Vittoria, L. Urbani, P. De Coppi, A. Olivo, Increased robustness and speed in low-dose phase-contrast tomography with laboratory sources, in: SPIE Optical Engineering + Applications, International Society for Optics and Photonics, 2016, pp. 996716-1–996716-10.
[174] P.C. Diémoz, F.A. Vittoria, C.K. Hagen, M. Endrizzi, P. Coan, A. Bravin, U.H. Wagner, C. Rau, I.K. Robinson, A. Olivo, A single-image retrieval method for edge illumination X-ray phase-contrast imaging: application and noise analysis, Phys. Med. 32 (12) (2016) 1759–1764.
[175] P. Diemoz, C. Hagen, M. Endrizzi, M. Minuti, R. Bellazzini, L. Urbani, P. De Coppi, A. Olivo, Single-shot X-Ray phase-contrast computed tomography with nonmicrofocal laboratory sources, Phys. Rev. Appl. 7 (4) (2017) 044029.
[176] A. Zamir, P.C. Diemoz, F.A. Vittoria, C.K. Hagen, M. Endrizzi, A. Olivo, Edge illumination X-ray phase tomography of multi-material samples using a single-image phase retrieval algorithm, Opt. Express 25 (10) (2017) 11984–11996.
[177] A. Olivo, S. Gkoumas, M. Endrizzi, C. Hagen, M. Szafraniec, P. Diemoz, P. Munro, K. Ignatyev, B. Johnson, J. Horrocks, et al., Low-dose phase contrast mammography with conventional X-ray sources, Med. Phys. 40 (9) (2013).
[178] P.C. Diemoz, A. Bravin, A. Sztrókay-Gaul, M. Ruat, S. Grandl, D. Mayr, S. Auweter, A. Mittone, E. Brun, C. Ponchut, et al., A method for high-energy, low-dose mammography using edge illumination X-ray phase-contrast imaging, Phys. Med. Biol. 61 (24) (2016) 8750.
[179] M. Marenzana, C.K. Hagen, P.D.N. Borges, M. Endrizzi, M.B. Szafraniec, K. Ignatyev, A. Olivo, Visualization of small lesions in rat cartilage by means of

laboratory-based X-ray phase contrast imaging, Phys. Med. Biol. 57 (24) (2012) 8173.

[180] M. Marenzana, C.K. Hagen, P.D.N. Borges, M. Endrizzi, M.B. Szafraniec, T.L. Vincent, L. Rigon, F. Arfelli, R.-H. Menk, A. Olivo, Synchrotron-and laboratory-based X-ray phase-contrast imaging for imaging mouse articular cartilage in the absence of radiopaque contrast agents, Philos. Trans. R. Soc. Lond. Ser. A 372 (2010) (2014) 20130127.

[181] K. Ignatyev, P. Munro, D. Chana, R. Speller, A. Olivo, Coded apertures allow high-energy X-ray phase contrast imaging with laboratory sources, J. Appl. Phys. 110 (1) (2011) 014906.

[182] A. Astolfo, M. Endrizzi, B. Price, I. Haig, A. Olivo, The first large-area, high-X-ray energy phase contrast prototype for enhanced detection of threat objects in baggage screening, in: SPIE Security + Defence, International Society for Optics and Photonics, 2016, pp. 999504-1–999504-7.

[183] M. Endrizzi, A. Astolfo, F.A. Vittoria, T.P. Millard, A. Olivo, Asymmetric masks for laboratory-based X-ray phase-contrast imaging with edge illumination, Sci. Rep. 6 (2016).

[184] M. Endrizzi, A. Astolfo, B. Price, I. Haig, A. Olivo, Asymmetric masks for large field-of-view and high-energy X-ray phase contrast imaging, J. Instrum. 11 (12) (2016) C12009.

[185] A. Astolfo, M. Endrizzi, F.A. Vittoria, P.C. Diemoz, B. Price, I. Haig, A. Olivo, Large field of view, fast and low dose multimodal phase-contrast imaging at high X-ray energy, Sci. Rep. 7 (2017).

[186] M. Endrizzi, B. Murat, P. Fromme, A. Olivo, Edge-illumination X-ray dark-field imaging for visualising defects in composite structures, Compos. Struct. 134 (2015) 895–899.

[187] M. Endrizzi, A. Astolfo, B. Price, I. Haig, A. Olivo, Large field-of-view asymmetric masks for high-energy X-ray phase imaging with standard X-ray tube, in: SPIE Optical Engineering + Applications, International Society for Optics and Photonics, 2016, pp. 99640A-1–99640A-6.

[188] C.K. Hagen, P. Maghsoudlou, G. Totonelli, P.C. Diemoz, M. Endrizzi, L. Rigon, R.-H. Menk, F. Arfelli, D. Dreossi, E. Brun, et al., High contrast microstructural visualization of natural acellular matrices by means of phase-based X-ray tomography, Sci. Rep. 5 (2015) 18156.

[189] P. Modregger, T.P. Cremona, C. Benarafa, J.C. Schittny, A. Olivo, M. Endrizzi, Small angle X-ray scattering with edge-illumination, Sci. Rep. 6 (2016).